TUDelft

Delft University of Technology

Single-Material Graphene Thermocouples

Harzheim, Achim; Könemann, Fabian; Gotsmann, Bernd; van der Zant, Herre; Gehring, Pascal

Important note
To cite this publication, please use the final published version (if applicable).
Please check the document version above.

Single-Material Graphene Thermocouples

Achim Harzheim, Fabian Könemann, Bernd Gotsmann, Herre van der Zant,
and Pascal Gehring**

**On-chip temperature sensing on a micro- to nanometer scale is becoming
more desirable as the complexity of nanodevices keeps increasing and
their downscaling continues. The continuation of this trend makes thermal
probing and management more and more challenging. This highlights the
need for scalable and reliable temperature sensors, which have the potential
to be incorporated into current and future device structures. Here, it is shown
that U-shaped graphene stripes consisting of one wide and one narrow leg
form a single material thermocouple that can function as a self-powering
temperature sensor. It is found that the graphene thermocouples increase in
sensitivity with a decrease in leg width, due to a change in the Seebeck coef-
ficient, which is in agreement with previous findings and report a maximum
sensitivity of $\Delta S \approx 39~\mu V~K^{-1}$.**

1. Introduction

Complex electronic devices and circuits rely on thermal sensors
incorporated into the structure to give input to the power and
thermal management system.[1,2] In order to avoid hot spots,
built-in temperature sensors are distributed along critical points
to monitor the temperature and provide feedback to the control
system.[3,4] This allows for the redistribution of the thermal load
through spot cooling or load distribution, for example, among
different computing cores, enabling a longer device lifetime
and saving energy. Ideally, these temperature sensors need to
have a small footprint, high accuracy, consume a minimum
amount of power and be compatible with established nano-
fabrication techniques. Today, resistors or diodes are often used
for on-chip temperature sensing, with diodes providing a high
sensitivity. However, since p-n junction diodes are made from
doped semiconductors they can be subject to fluctuations in the
doping and have to be calibrated individually.

A. Harzheim, Dr. P. Gehring
Department of Materials
University of Oxford
Oxford OX2 6HT, United Kingdom
E-mail: achim.harzheim@materials.ox.ac.uk; pascal.gehring@imec.be
Dr. F. Könemann, Dr. B. Gotsmann
IBM Research – Zurich
Rueschlikon 8803, Switzerland
Prof. H. van der Zant, Dr. P. Gehring
Kavli Institute of Nanoscience
Delft University of Technology
Delft 2628, Netherlands

Thermocouples are another tempera-
ture monitoring option, which is widely
used if sensing is required due to their
simplicity and reliability.[5] Thermocou-
ples are relatively easy to fabricate and
are self-powered making them an ideal
candidate for low-cost thermometry, since
their signal stems from intrinsic mate-
rial properties, they tend to have only
minimal variations in sensitivity. As the
name suggests, a thermocouple, in the
classical sense, is typically a combination
of two materials (often metals) with dif-
ferent Seebeck coefficients $S = -\Delta V/\Delta T$,
which are joined at the sensing end.[6]
Then a temperature difference between
the sensing end at T_{sense} and the meas-
uring end at T_{meas} leads to the buildup of a thermovoltage via
the Seebeck effect:

$$V_{\text{th}} = -\left[(S_1 - S_2)(T_{\text{sense}} - T_{\text{meas}})\right] \tag{1}$$

where V_{th} refers to the thermovoltage drop across the two leads
at the measuring end and S_1 and S_2 are the Seebeck coefficients
of the two materials used. Depending on the desired working
temperature range and the required sensitivity different mate-
rial combinations are used. A multitude of different types of
thermocouples has been developed, covering a wide range of
temperatures and work environments.[7–10] Typically, in order
to achieve on-chip thermometry with conventional thermocou-
ples, two separate fabrication runs are required.

It has previously been shown that it is possible to produce a
single-material thermocouple by varying the width of thin gold
stripes[11,12] and other metals.[13] The proposed mechanism is
that reducing the width of the gold stripes changes the Seebeck
coefficient due to increased scattering at the grain boundaries
and structural defects. However, the sensitivity of all-metal ther-
mocouples is only on the order of $1~\mu V~K^{-1}$ and they tend to
have a large footprint of tens of μm in width and hundreds of
μm in length, which is too big for nanoelectronic applications.
In addition, their thickness on the order of 100 nm makes it
challenging to integrate them vertically in nanoelectronic
devices. Here, we report the fabrication of 2D thermocouples
made out of single layer graphene. To this end, we make use of
our recent discovery that similar to metals, the Seebeck coeffi-
cient in graphene can be influenced by geometrical constraint,
which changes the mean free path locally.[14] The advantage of
using graphene compared to previous approaches is its high
bulk Seebeck coefficient[15] and its long electron mean free
path even at room temperature.[16] This allows for the fabrica-
tion of highly sensitive thermocouples with the possibility of

**ADVANCED
SCIENCE NEWS**
www.advancedsciencenews.com

**ADVANCED
FUNCTIONAL
MATERIALS**
www.afm-journal.de

wafer-scale integration, as current research efforts are directed at the use of graphene in 2D van der Waals structures using wafer-scale fabrication methods.[17,18]

2. Results and Discussion

The graphene thermocouples are fabricated by patterning a U-shape into CVD-grown graphene consisting of a wide and a narrow leg. To test the functionality of the thermocouples, an on-chip microheater is used to increase the temperature of the sensing end of the thermocouple (see **Figure 1**a). We fabricate both long (L_1 = 4.3 µm) and short (L_2 = 2.5 µm) thermocouples and vary the width of the narrow leg w from 1 µm to 0.2 µm while keeping the width of the wide leg constant at w_0 = 1.5 µm. The sensing end of the thermocouple where the wide and narrow legs meet is located 700 nm from the heater.

We use a scanning thermal microscope (SThM) to calibrate the heater and quantify the temperature distribution along the device. To this end we performed an SThM measurement of the device structure at different heater currents and obtain a temperature profile map of the device (see Figure 1b). We used
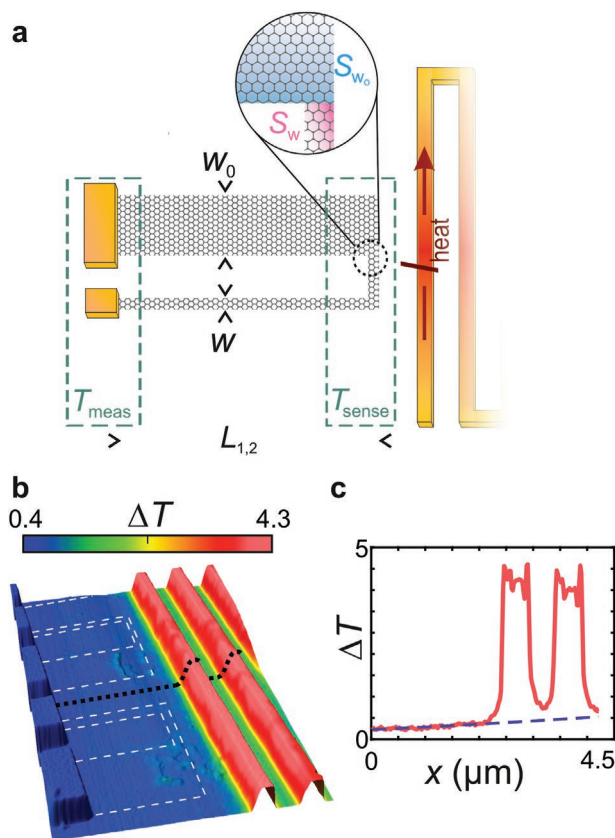
Figure 1. a) Schematic depiction of the device structure. b) Temperature distribution of a typical operating device measured using SThM at a heater power of 6.4 mW. The white dashed lines indicate the position of the graphene thermocouples and the black dashed line indicates the line cut shown in (c). c) Temperature profile line extracted from (b) in pink and the fit along the substrate (blue dashed line).
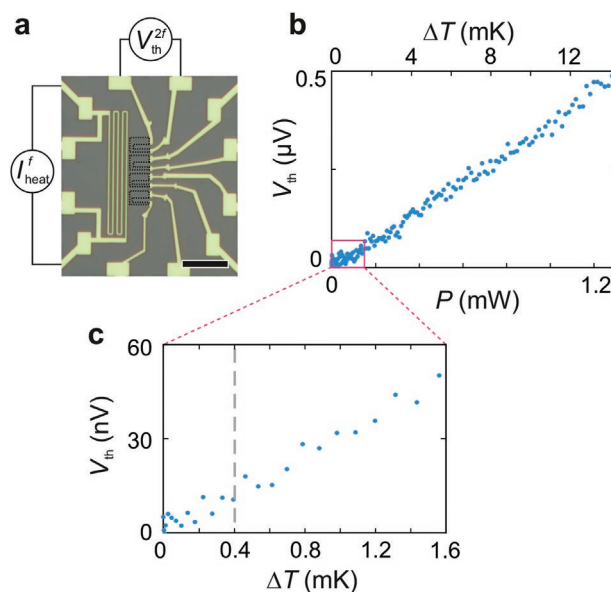
Figure 2. a) Optical microscope image of a typical device showing the measurement configuration. The graphene thermocouples next to the heater are highlighted by the black dotted lines and the scale bar denotes 10 µm. b–c) Thermovoltage response of a short device with w = 0.2 µm to heater power, the blow-up below shows the same measurement with higher integration time where the grey dashed line indicates the minimum temperature sensitivity.

a method that eliminates the influence of fluctuations in the tip sample thermal resistance.[19,20] This enabled us to develop a model for the temperature gradient along the substrate and subsequently calculate the temperature difference $\Delta T = T_{sense} - T_{meas}$ (see Figure 1c and Supporting Information).

In order to quantify the sensitivity of the thermocouple, the heater is excited with a sinusoidal current at a frequency f and the thermovoltage response of the thermocouple is recorded at a frequency $2f$ between the wide and narrow leg (see **Figure 2**a). For the purpose of this paper, all signals reported are the phase independent root-mean-square (RMS) values though the thermovoltage signal is mainly present at a phase of 90° with respect to the excitation.[21] Since we aim to determine the peak value of the thermovoltage response, the measured RMS signal is multiplied by a factor of $\sqrt{2}$. The resistance of the devices is extracted from a DC IV trace, with all measured devices exhibiting a linear behavior (see Supporting Information). Measurements are performed at room temperature and in a vacuum environment to prevent parasitic heat transfer due to conduction and convection.

As is shown in Figure 2b, for the best performing device geometry, which is a short junction with a narrow leg width of w = 0.2 µm (see analysis below), the junction responds linearly to the heater power P. Assuming that the temperature difference is proportional to the heater power, the observed behavior is in agreement with the Joule–Lenz law which predicts a quadratic relation between the heating power P and the applied current I, $\Delta T = T_{sense} - T_{meas} \propto P = I^2 R$. A higher heater power will induce a higher temperature difference ΔT which results in a higher thermovoltage signal, see Equation (1). Using the SThM

calibration allows us to convert the heater power P into a corresponding temperature drop ΔT on the junction, which we show as a top x-axis in Figure 2b.

A clear increase in the thermovoltage signal is seen for relatively small temperature differences of a few mK. For a longer integration time (10 s compared to 1 s for Figure 2b) it is possible to push the response threshold to an even smaller temperature difference of $\Delta T \approx 400$ μK (see Figure 2c grey dashed line) highlighting the excellent sensing abilities of the graphene thermocouples: a maximum sensitivity of $\Delta S \approx 39$ μ V K^{-1} is reached for a width of $w = 0.2$ μm and a length of $L_2 = 2.5$ μm.

The origin of the signal can be explained by a change in the Seebeck coefficient (S_{w_0} to S_w) when varying the leg width from $w_0 = 1.5$ μm to a narrower width w.[14] This change in the Seebeck coefficient is due to the increased influence of scattering from the edges on the mean free path as the width of the channel is reduced. As scattering is more prominent in the narrow channel the mean free path decreases. Here, the defect potentials responsible for the scattering stems from irregularities at the edges in the graphene devices, introduced by the oxygen plasma etching necessary to pattern the devices as well as atmospheric contamination.

Following a previously developed theory for CVD graphene in the diffusive transport regime[14] it is then possible to arrive at a width dependent expression for the mean free path

$$l(w) = l_0 \left[1 + c_n \left(\frac{l_0}{w} \right)^n \right]^{-1} \tag{2}$$

where l_0 is the bulk mean free path and c_n and n are numerical coefficients specifying the transport mode and the influence of scattering on the mean free path. We can then combine Equation (2) with the Mott formula for the Seebeck coefficient given by $S = -\frac{\pi^2 k_B^2 T}{2e} \frac{1}{R(\epsilon)} \frac{dR(\epsilon)}{d\epsilon} \Big|_{\epsilon = \epsilon_F}$, where $R(\epsilon)$ is the energy dependent resistance in graphene. While the Seebeck coefficient of graphene can deviate from the Mott formula at high temperatures, the Mott formula gives a good indication of the signal and has been shown to reproduce the trend in experimental data correctly.[15] Using the Mott formula results in an expression for the width dependent Seebeck coefficient in graphene

$$S = -\frac{\pi^2 k_B^2 T}{2\epsilon_F e} \left[1 + nU \frac{l(w)}{l_0} - (n-1)U \right] \tag{3}$$

Here, $U = \frac{d \ln(l_0)}{d \ln(\epsilon)} \Big|_{\epsilon = \epsilon_F}$ is the exponent of any power law dependence of the electron mean free path on energy and $\epsilon_F = \hbar v_F \sqrt{\frac{4\pi n}{g_s g_v}}$ is the Fermi energy with the Fermi velocity $v_F = 10^6$ m s^{-1}, the spin and valley degeneracy $g_s = g_v = 2$ and $n = 10^{16}$ m^{-2} being the carrier density.[22] Equation (3) predicts a decrease in thermopower as the width of the graphene channel is reduced. This means that the difference ΔS between S_{w_0} and S_w (see Figure 1a) is expected to be largest for narrow w. The Seebeck coefficient difference ΔS can thus be expressed as
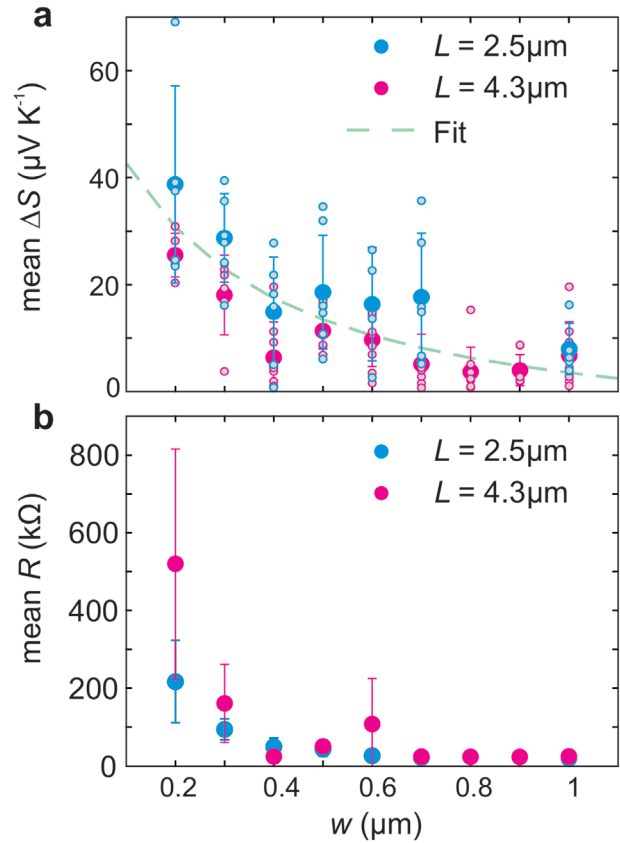
Figure 3. a) Mean ΔS signal as a function of the narrow leg width w for long $L_1 = 4.3$ μm (red dots) and short $L_2 = 2.5$ μm (blue dots) devices respectively. The grey dots indicate single device measurements for the long (red outline) and short devices (blue outline) respectively and the error bars indicate the standard deviation with respect to these single measurements. The green dashed line is the fit using Equation (4). For the short length devices, the widths $w = 0.9$ μm and $w = 0.8$ μm could not be measured due to a fabrication error. b) Average device resistance for the short (blue dots) and long (red dots) devices as a function of the narrow leg width w, where the errorbars indicate the standard deviation.

$$\Delta S = S_{w_0} - S_w = -\frac{\pi^2 k_B^2 T n U}{3\epsilon_F e} \left[\frac{l(w_0) - l(w)}{l_0} \right] \tag{4}$$

Usually the Seebeck coefficient S is temperature dependent, however for the small temperature gradients used in our study we can assume that $S_w(T_{sense}) \approx S_w(T_{meas})$ and similarly for S_{w_0}.

The width dependence of both the ΔS signal and the resistance for over 110 devices with differing widths w from 1 to 0.2 μm is shown in **Figure 3** for the two different device lengths L_1 and L_2. The thermovoltage was recorded at a heater power of $P \approx 1.3$ mW for all devices. This corresponds to a temperature difference between the sensing end and the measuring end of $\Delta T_{short} = 14.3 \pm 2.17$ mK for the short devices and $\Delta T_{long} = 22.35 \pm 2.97$ mK for the long devices. As the narrow leg width decreases, the mean ΔS increases, in accordance with Equation (4), which predicts that a lower mean free path in the narrow leg will lead to a higher Seebeck difference ΔS

(Figure 3a). Similarly, the resistance of both the long and short devices increases with decreasing width w (Figure 3b).

The increase in resistance (of Figure 3b) can be explained by the same formalism used to describe the thermoelectric properties of the system, where the CVD graphene on SiO_2 is treated as a diffusive conductor.[23] In the diffusive transport regime, the conductance is proportional to the electron mean free path, $\sigma \propto l_e$. Since $\sigma \propto 1/R$ we then expect $l_e \propto 1/R$, meaning an increase in resistance for a smaller electron mean free path. This can be seen in Figure 3b where a narrowing leg width w reduces the mean free path due to scattering along the rough edges resulting in a higher resistance R.

As the mean free path is the crucial factor in determining the resistance and equally the determining factor for ΔS (see Equation (4)), a decrease in the resistance should simultaneously show up as a decrease in the ΔS signal and vice versa. This is evident in Figure 3a,b for the long devices, where small variations in the device resistance when changing w from 0.5 to 0.4 µm are directly reflected in corresponding variations of the ΔS signal.

Both the long, $L_1 = 4.3$ µm, and the short, $L_2 = 2.5$ µm, devices show a similar trend of an increasing ΔS signal with a decreasing channel width (Figure 3a). The ΔS signal for both device lengths can be fitted using Equation (4), accounting for the different ΔT and using the same fitting parameters for both lengths (see Figure 3a black dashed line). We find $c_n = 0.96$, $l_0 = 248$ nm, $n = 1.08$ and $U = 0.99$, which is similar to previously found values from measurements of the thermopower width dependence in CVD grown graphene.[14] The U value of ≈1 points toward long-range Coulomb interaction being the determining factor in the mean free path, consistent with scattering centres along the graphene edges.[24,25] Differences in signal strength between the long and short devices, as well as for individual devices (see Figure 3a), can be attributed to the unpredictable nature of the defects in the narrow graphene legs, ultimately determining the size of S_w. In addition, effects steming from grain boundaries or singlelayer/bilayer junctions could contribute to the sample-to-sample variation observed in our experiments (and quantified by the error bars in Figure 3a). This leads to a relatively high standard deviation for the ΔS signals in the graphene thermocouples, however we note that the Seebeck response of the short and long devices are within one standard deviation of each other.

It should be noted that the critical dimensions of the graphene thermocouples are w_0 and w. Ideally w_0 should be larger than the mean-free path in the graphene to avoid influence from edge scattering, while w should be as small as possible to maximize edge scattering. The minimum size of $w = 0.2$ µm in this study is due to limitations in our fabrication process. Furthermore, an avenue to achieve more sensitive thermocouples is to increase the "bulk" value S of graphene, which can be achieved by oxygen plasma treatment of graphene,[26] operating in the hydrodynamic regime,[27] encapsulating graphene in hBN[16,28] as well as changing the carrier concentration and band structure through gating.[15,29] Another possible path is to use exfoliated graphene which has a higher electron mean free path and therefore a higher Seebeck coefficient than CVD grown graphene[30] and in addition exhibits less defects than CVD graphene, making it easier controllable. However, similar to most of the other enhancement approaches mentioned above, the drawbacks are limited scalability of the graphene thermocouples due to a progressively more complex fabrication process. Nonetheless, an improved control over the edge configuration in graphene and therefore edge scattering and the mean free path is needed and further advances as well as more sophisticated fabrication methods should enable the creation of reproducible and well-defined thermocouples.[31,32]

3. Conclusion

In summary, we developed a single material thermocouple consisting of a U-shaped graphene structure with a narrow and a wide leg joined at the temperature sensing end. The behavior of the thermocouple is well modeled by a previously developed theory on the dependence of the thermoelectric properties of graphene on its geometry. Furthermore, we demonstrated a higher sensitivity than in previously reported single material thermocouples by well over an order of magnitude at a footprint of only a few micrometers in width and length. The devices presented in this study thus could be used to facilitate cheap and easy to fabricate on-chip thermometry while being compatible with van der Waals heterostructures, current MOSFETs and future graphene circuits. In addition, due to the bioinert nature of graphene,[33] as well as the small footprint and sub-millikelvin sensitivity of the graphene thermocouples they lend themselves to the increasingly relevant task of temperature probing of cells and other living systems.[34,35]

Conflict of Interest

The authors declare no conflict of interest.

[1] K. Skadron, M. R. Stan, W. Huang, S. Velusamy, K. Sankaranarayanan, D. Tarjan, *IEEE Micro* **2003**, *23*, 52.

[2] S. H. Gunther, in *IEEE Topical Meeting on Electrical Performance of Electronic Packaging*, IEEE, Piscataway, NJ **2001**, pp. 7–8.

[3] O. Semenov, A. Vassighi, M. Sachdev, *IEEE Trans. Device Mater. Reliab.* **2006**, *6*, 17.

[4] R. Mukherjee, S. O. Memik, in *Proc. of the 43rd annual Design Automation Conference*, ACM Press, New York **2006**, pp. 542–547.

[5] J. Machin, D. Tucker, J. V Pearce, *Meas. Sci. Technol.* **2018**, *29*, 067002.

[6] P. A. Kinzie, L. G. Rubin, *Phys. Today* **1973**, *26*, 52.

[7] M. A. Kazemi, D. S. Nobes, J. A. W. Elliott, *Langmuir* **2017**, *33*, 7169.

[8] R. R. Asamoto, P. E. Novak, *Rev. Sci. Instrum.* **1967**, *38*, 1047.

[9] I. M. Tougas, M. Amani, O. J. Gregory, *Sensors* **2013**, *13*, 15324.

[10] D. D. Pollock, *Thermocouples: Theory and Properties*, CRC Press, Boca Raton, FL **1991**, p. 324.

[11] W. Sun, H. Liu, W. Gong, L.-M. Peng, S.-Y. Xu, *J. Appl. Phys.* **2011**, *110*, 083709.

[12] H. Liu, W. Sun, S. Xu, *Adv. Mater.* **2012**, *24*, 3275.

[13] G. P. Szakmany, A. O. Orlov, G. H. Bernstein, W. Porod, *IEEE Trans. Nanotechnol.* **2014**, *13*, 1234.

[14] A. Harzheim, J. Spiece, C. Evangeli, E. McCann, V. Falko, Y. Sheng, J. H. Warner, G. A. D. Briggs, J. A. Mol, P. Gehring, O. V. Kolosov, *Nano Lett.* **2018**, *18*, 7719.

[15] Y. M. Zuev, W. Chang, P. Kim, *Phys. Rev. Lett.* **2009**, *102*, 096807.

[16] L. Banszerus, M. Schmitz, S. Engels, M. Goldsche, K. Watanabe, T. Taniguchi, B. Beschoten, C. Stampfer, *Nano Lett.* **2016**, *16*, 1387.

[17] K. Zhang, F. L. Yap, K. Li, C. T. Ng, L. J. Li, K. P. Loh, *Adv. Funct. Mater.* **2014**, *24*, 731.

[18] A. Avsar, T. Y. Yang, S. Bae, J. Balakrishnan, F. Volmer, M. Jaiswal, Z. Yi, S. R. Ali, G. Guöntherodt, B. H. Hong, B. Beschoten, B. Özyilmaz, *Nano Lett.* **2011**, *11*, 2363.

[19] F. Menges, P. Mensch, H. Schmid, H. Riel, A. Stemmer, B. Gotsmann, *Nat. Commun.* **2016**, *7*, 10874.

[20] F. Könemann, M. Vollmann, T. Wagner, N. Mohd Ghazali, T. Yamaguchi, A. Stemmer, K. Ishibashi, B. Gotsmann, *J. Phys. Chem. C* **2019**, *123*, 12460.

[21] P. Gehring, M. Van Der Star, C. Evangeli, J. J. Le Roy, L. Bogani, O. V. Kolosov, H. S. J. Van Der Zant, *Appl. Phys. Lett.* **2019**, *115*, 073103.

[22] S. Das Sarma, S. Adam, E. H. Hwang, E. Rossi, *Rev. Mod. Phys.* **2011**, *83*, 407.

[23] S. Adam, E. H. Hwang, V. M. Galitski, S. Das Sarma, *Proc. Natl. Acad. Sci. USA* **2007**, *104*, 18392.

[24] A. H. Castro Neto, F. Guinea, N. M. R. Peres, K. S. Novoselov, A. K. Geim, *Rev. Mod. Phys.* **2009**, *81*, 109.

[25] Q. Li, S. Das Sarma, *Phys. Rev. B: Condens. Matter Mater. Phys.* **2013**, *87*, 085406.

[26] N. Xiao, X. Dong, L. Song, D. Liu, Y. Tay, S. Wu, L. J. Li, Y. Zhao, T. Yu, H. Zhang, W. Huang, H. H. Hng, P. M. Ajayan, Q. Yan, *ACS Nano* **2011**, *5*, 2749.

[27] F. Ghahari, H. Y. Xie, T. Taniguchi, K. Watanabe, M. S. Foster, P. Kim, *Phys. Rev. Lett.* **2016**, *116*, 136802.

[28] J. Duan, X. Wang, X. Lai, G. Li, K. Watanabe, T. Taniguchi, M. Zebarjadi, E. Y. Andrei, *Proc. Natl. Acad. Sci. USA* **2016**, *113*, 14272.

[29] C. R. Wang, W. Sen Lu, L. Hao, W. L. Lee, T. K. Lee, F. Lin, I. C. Cheng, J. Z. Chen, *Phys. Rev. Lett.* **2011**, *107*, 186602.

[30] K. S. Novoselov, V. I. Fal'ko, L. Colombo, P. R. Gellert, M. G. Schwab, K. Kim, *Nature* **2012**, *490*, 192.

[31] K. He, G. Do Lee, A. W. Robertson, E. Yoon, J. H. Warner, *Nat. Commun.* **2014**, *5*, 3040.

[32] X. Zhang, O. V. Yazyev, J. Feng, L. Xie, C. Tao, Y. C. Chen, L. Jiao, Z. Pedramrazi, A. Zettl, S. G. Louie, H. Dai, M. F. Crommie, *ACS Nano* **2013**, *7*, 198.

[33] Y. Shao, J. Wang, H. Wu, J. Liu, I. A. Aksay, *Electroanalysis* **2010**, *22*, 1027.

[34] G. Kucsko, P. C. Maurer, N. Y. Yao, M. Kubo, H. J. Noh, P. K. Lo, H. Park, M. D. Lukin, *Nature* **2013**, *500*, 54.

[35] T. Bai, N. Gu, *Small* **2016**, *12*, 4590.